A proxy of subsurface Chlorophyll-a in shelf waters: use of density profiles and the below mixed layer depth (BMLD)

Arianna Zampollo[1,*], Thomas Cornulier[1], Rory O'Hara Murray[2], Jacqueline Fiona Tweddle[1], James Dunning[1], Beth E. Scott[1]

[1] School of Biological Sciences, University of Aberdeen, Aberdeen, AB24 2TZ, UK

[2] Marine Scotland Science, Aberdeen, AB11 9DB, UK

Correspondence to: Arianna Zampollo (zampolloarianna@gmail.com)

Abstract

Primary production dynamics are strongly associated with vertical density profiles in shelf waters. Climate change and artificial structures (e.g. windfarms) are likely to modify the strength of stratification and the vertical distribution of nutrient fluxes, especially in shelf seas where the balance between mixing and stratification defines the vertical distribution of phytoplankton. To understand the effect of physical changes on primary production, identifying the linkage between density and chlorophyll-a (Chl-a) profiles is essential. Here, the biological relevance of eight density levels (DLs) characterizing three different portions of the pycnocline (start, centre, end) was evaluated to find a valuable proxy for subsurface Chl-a concentrations in stratified conditions. The vertical distribution of Chl-a maximum (CMd) was compared to the depth of DLs by hypothesizing their occurrence at the same depth using Spearman correlation, linear regression, and a Major Axis analysis. Out of 1237 observations of the water column exhibiting a pycnocline, 78% reported CMd above the base of the pycnocline (BMLD) with an average distance equal to 2.74 ± 5.21 m. BMLD appeared as a vertical boundary up to which subsurface Chl-a maxima distribute in shallow waters (depth ≤ 115 m), suggesting a significant contribution of deep mixing processes in supporting subsurface production under specific conditions (stratification and bathymetry). Here, we describe and advise BMLD as a valuable tool for understanding the spatiotemporal variability of Chl-a in shelf seas, and provide a method, and a function, to extrapolate it from density profiles.

Keywords

BMLD, CMd, deep mixing, MLD, pycnocline, SCML, shelf sea

1. Introduction

As we begin to manage our oceans and shelf seas for more complex simultaneous uses, such as renewable energy developments, fishing and marine protected areas, it is becoming increasingly important understanding details of primary productivity at fine spatial scales. Besides very shallow waters, the vast majority of phytoplankton in continental shelf waters generally grows under stratified conditions, where the pycnocline acts as a barrier against the mixing of the whole water column and allows cells to buoyance and photosynthesize within the euphotic zone. The balance between stratification and mixing in the water column is determinant for phytoplankton, and, in the North Sea, it fluctuates in time and space by the modulation of daily and biweekly strong tidal cycles (Klymak et al., 2008). Turbulent mixing of the water column requires energy sources from either the surface (e.g. wind stress, Ekman pump due to wind curl) or deep waters (e.g. upwelling, eddy diffusion, tidal currents), which can be altered by climate change and man-made infrastructures (Dorrell et al., 2022). Therefore, changes are expected in the overall mixing budget of our seas. Anomalies as circulation slow-down, sea-level rise, bottom and surface temperature, wind speed and wave height have largely been described as a consequence of climate change in the last two decades (e.g. Orihuela-Pinto et al., 2022; Taboada and Anadón, 2012; Bonaduce et al., 2019), while the consequences of these changes on the biological processes are still partially understood (Lozier et al., 2011; Somavilla et al., 2017).

1.1 Subsurface chlorophyll-a maxima layers (SCMLs)

Many of the uncertainties regarding the impacts on primary production come from the difficulties in sampling the community composition and the total abundance throughout the whole water column. Contrary to the detection of surface blooms by satellite sensors, subsurface chlorophyll-a maxima layers (SCMLs) are often more difficult to describe and measure. SCMLs represent significant features in plankton systems (Cullen, 2015), they define where most of the bottom-up processes take place and can encompass more than 50% of the entire water column production (Weston et al., 2005; Takahashi and Hori, 1984). In the North Sea, the summertime (May-August) subsurface production contributes to the annual production of up to 20-50% and sustain the food chain in continental shelf waters during prolonged stratified conditions (Hickman et al., 2012; Richardson and Pedersen, 1998; Weston et al., 2005). Several studies linked the vertical distribution of maximum chlorophyll-a (Chl-a) to deep mixing processes (e.g. Brown et al., 2015; Richardson and Pedersen, 1998; Sharples et al., 2006; Zhao et al., 2019b) and identified the occurrence of deep Chl-a assemblages in the proximity of the pycnocline in shelf seas (e.g. Costa et al., 2020; Durán-Campos et al., 2019; Ross and Sharples, 2007; Sharples et al., 2001). The stratification is generally controlled by mixing processes (tidal mixing and surface wind stress) and sources of buoyancy (surface heating and estuarine inputs of low salinity), whose balance allow primary producers to grow in favourable light and nutrient conditions within the pycnocline. In the North Sea, mixing processes are mostly regulated by strong tidal currents (Glorioso and Simpson, 1994; Loder et al., 1992; Sharples et al., 2006, 2001; Simpson et al., 1980; Zhao et al., 2019b), especially in prolonged stratified conditions, when upward fluxes represent the only source of nutrients intake within the pycnocline. Maxima Chl-a have been identified at the base of the pycnocline in regions of strong tidal mixing at Georges Bank in August (Holligan et al., 1984) and within the western English Channel (Sharples et al., 2001). However, despite the clear linkage between SCMLs and tidal mixing in shelf seas, variations on productivity have been mainly conducted at oceanic sites by investigating the mixing processes above the pycnocline (within the upper mixed layer) (Somavilla et al., 2017; Steinacher et al., 2010), omitting the effects of processes close to the seabed, e.g. variations of mixing processes below the pycnocline. On the other hand, studies on shelf waters suggest variations of the water column due to both surface and deep mixing processes, since the interplay of marine components from surface to seabed are more adjacent than in deep oceanic locations (Durski et al., 2004).

1.2 Mixed layer depth (MLD) and pycnocline characteristics

MLD has been largely considered as a central variable for understanding phytoplankton dynamics (Sverdrup, 1953), especially in oceanic sites, where several studies have investigated the ecological relevance of MLD on Chl-a vertical distribution (Behrenfeld, 2010; Carranza et al., 2018; Diehl, 2002; Diehl et al., 2002; Gradone et al., 2020), phytoplankton bloom events (Behrenfeld, 2010; Chiswell, 2011; D'Ortenzio et al., 2014; Prend et al., 2019; Ryan-Keogh and Thomalla, 2020, Sverdrup, 1953), and the effects of climate change (Somavilla et al., 2017). The nutricline's depth exhibits positive correlations with the upper mixed layer depth (Ducklow et al., 2007; Gradone et al., 2020; Holligan et al., 1984; Prézelin et al., 2000, 2004; Ryan-Keogh and Thomalla, 2020; Yentsch, 1974, 1980), and it has been generally associated with surface spring blooms or windstorm events (e.g. Banse, 1987; Carranza et al., 2018; Carvalho et al., 2017; Lande and Wood, 1987; Therriault et al., 1978). However, the effect of climate change on MLD and primary production is still an unsolved question (Lozier et al., 2011; Somavilla et al., 2017). The need for a much more detailed understanding of the linkage between primary production, pycnocline characteristics and deep turbulent processes (below the pycnocline) is therefore a key area of research, especially in highly productive but spatially heterogeneous areas such as shelf waters and shallow seas.

The methods for identifying MLDs vary among marine environments, hydrodynamic regimes, or the spatial resolution of vertical profiles (Courtois et al., 2017; Lorbacher et al., 2006), because making use of a single method is difficult for spatiotemporally heterogeneous regions. MLDs are typically defined as the depth at which the density exceeds a specific value (threshold) (e.g. Kara et al., 2000), however this method presents issues in specific hydrodynamic conditions, such as over estimating MLD in regions with deep convection (e.g. subpolar oceans) (Courtois et al., 2017), or misidentifying water columns with a newly established shallow MLD over previous periods of stratification (Somavilla et al., 2017). Several sensitivity tests and comparisons have been conducted in oceanic waters (e.g. Carvalho et al., 2017; Courtois et al., 2017; González-Pola *et al.*, 2007; Holte and Talley, 2009), however, there are no standard methods for MLD identification neither in shelf nor oceanic waters.

1.3 A new way forward: the base of the pycnocline (BMLD) as a proxy for Chl-a maximum in shelf waters

In this study, we proposed the adaptation of existing methods into a new algorithm able to cope with different high-resolution (1 m) vertical distributions of density (therefore being able to deal with split pycnoclines and unusual shapes) to characterize the depth between the pycnocline and i) the surface mixed layer (commonly known as "MLD", here renamed as above mixed layer depth, AMLD) and ii) the below mixed layer depth (BMLD). The method is validated in waters depths from 20 to 120 m, with 14 years of repeated surveys that covers a mosaic of habitats types: seasonal stratified waters, permanently mixed waters, regions of freshwater inputs and strong tidal mixing (Leeuwen et al., 2015). The vertical distribution of density and Chl-a profiles are compared and the biological relevance of BMLD in investigating subsurface Chl-a is detailed. This approach is being developed in order to help the identification of key linkages between the physical environment and primary production at finer spatial scales (punctual location up to $\leq$ 1 km), which can be ecologically relevant for pressing issues in marine spatial management (e.g. seabed leasing for wind farms, locations of MPAs) and spatially explicit climate change assessments.

2. Methods

Vertical samples of density and Chl-a (see Sect. 2.1) were used to characterize the relationship between stratification features (see Sect. 2.2 and 2.3) and subsurface Chl-a (described as abundance and vertical distribution, see Sect. 2.4). The most frequent methods used to identify vertical characteristics of density profiles (density levels – DLs) (see Sect. 2.3)

were compared to the proposed algorithm estimating the above and below limits of the pycnocline (AMLD and BMLD, Sect. 2.2). Here, a new method to identify BMLD is proposed, and its potential is evaluated by comparing it with the vertical distribution of subsurface Chl-a during spring and summer (April-August) (see Sect. 2.5).

2.1 Physical and biological oceanographic samples

In situ summertime measurements of temperature, salinity, and Chlorophyll-a (Chl-a) were collected from a towed, undulating, CTD and a vertical CTD in the North Sea off the East coast of Scotland, UK, within the Firth of Forth (FoF) and Tay region for over 14 years (from 2000 to 2014) (Fig. 1). A total of 1273 profiles from both types of sampling were extracted from April to August (April=3, May=51, June=1115, July=66, August=38). 426 profiles were gathered using the vertical CTD from 12 oceanographic campaigns carried out by Marine Scotland Science on board of the fisheries research vessels *Scotia* and *Alba na Mara* (www.gov.scot/marine-and-fisheries). The data set comprises temperature, conductivity, and Chl-a measurements from the sea surface to the seabed (vertical resolution equals to 1 decibar) at fixed stations sites. Water samples were collected during each cast for calibration of the *in situ* sensor data. The undulating CTD sampled the water column in June 2003 and July 2014 with a continuous vertical and horizontal oscillation of the instrument throughout the water column from 2-5 m below the sea surface to 5 m from the seabed. The continuous profiles obtained from undulating CTD were converted into 847 single profiles of the water columns. Data were sampled at 1 second intervals, resulting in a vertical resolution comprising between 0.5 and 1 m, in water depths from 25 m to 115 m. More information about the oceanographic cruise in June 2003 are described in Scott et al. (2010), whose method was used also in July 2014.
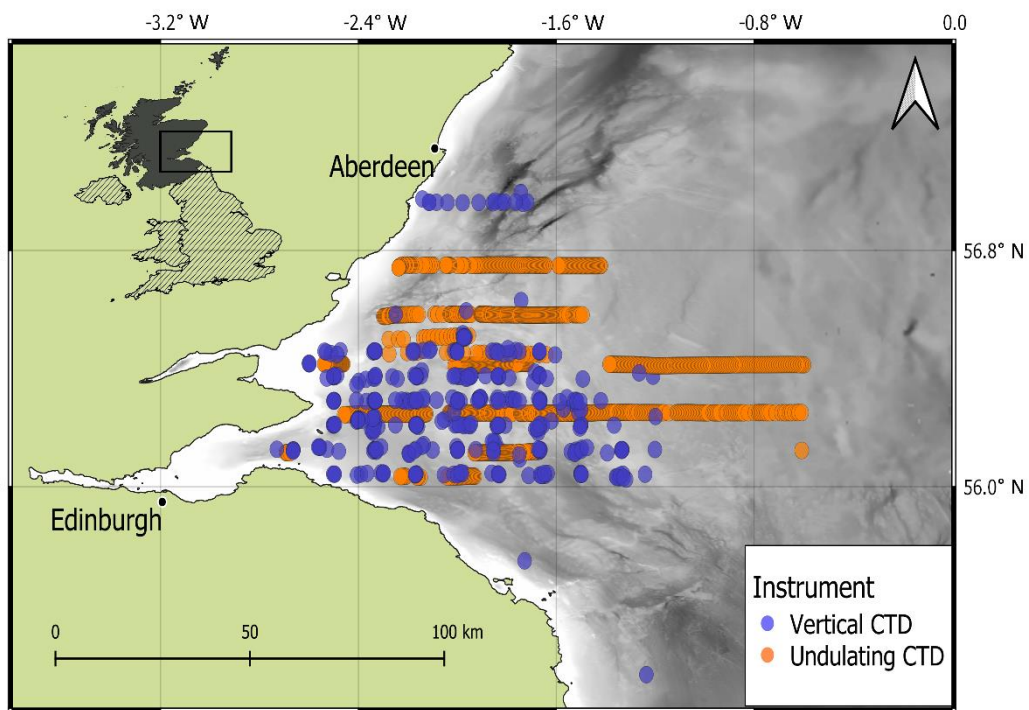
Figure 1: Study area with the in situ surveys measured by an undulating CTD (orange dots) and a vertical CTD (blue dots). Land (green) and bathymetry (grey colour ramp) are pictured (ESRI 2020; EMODnet 2018)

2.1.1 Standardized density profiles

Since the proposed algorithm (described in Sect. 2.2) works with profiles at high vertical resolution (samples' vertical resolution is 1 m), the *in situ* casts must be standardized throughout the water column. Density (ρ) observations taken every 0.5 to 1 m from undulating CTD were converted into measurements over regular depth intervals by smoothing and interpolating. This was achieved by fitting a generalized additive model (GAM) (Hastie and Tibshirani, 1990) using an adaptive spline with ρ as a function of depth. The smoothing basis (knots) were selected in a range from 75% to 90% of the number of observations occurring within each profile. The obtained smooth function for each profile was used to interpolate ρ at regular 1 m depth intervals. In order to maintain the same shape and values in each profile, the fitted curves at 1 m interval were visually checked by plotting the estimated and real profiles to visually identify possible errors. 4.16% of the shapes (*n*=53) were manually corrected by changing the number of knots in the GAM. An example is given at Figure A2 in Appendix A. The analyses were run in R v3.6.3 (R Core Team, 2018) using the *mgcv* v1.8-33 package.

2.2 AMLD and BMLD detection

Definition of AMLD and BMLD

In stratified waters, the layers above and below the pycnocline are mixed vertical region where the density gradient is significantly different from the pycnocline. The surface mixed layer depth (AMLD) and the mixed layer depth below the pycnocline (BMLD) are both transitional layers from a mixed to a stratified vertical region occurring at the beginning and end of the pycnocline. The most common threshold methods (see Sect 2.3) identify AMLD based on the principle that the mixed layer at the surface has a density's variance close to zero, which separates from the pycnocline, exhibiting a larger density gradient. The above assumptions may not always hold, especially when the upper mixed layer is heterogeneous with nested sub-structures such as small re-stratification at the surface, or when the pycnocline can include a small mixed layer (Fig. A1a, e, f in Appendix A) or presents different density gradients (stratified layers) within it (Fig. A1b and c in Appendix A). Such density conditions are difficult to isolate with the available methods.

In the proposed algorithm, the detection of AMLD does not assume that the mixed layer has a density gradient close to zero, and it identifies MLDs regardless any *a priori* threshold. It also picks up the shallowest and deepest limits of the pycnocline by excluding middle breaks of the pycnocline, allowing the identification for unconventional density vertical distribution. The definition of AMLD and BMLD are based on common conventions: small and similar $\Delta\rho$ (measured as the difference between two consecutive points, $\Delta\rho_z = |\rho_z - \rho_{z+1}|$) within the mixed layers and within the pycnocline; the pycnocline is enclosed by layers of mixed water above and/or below it exhibiting a different $\Delta\rho$; the mixed layer depth is pinpointed independently from a fixed gradient (Chu and Fan, 2019, 2011; Holte and Talley, 2009). The AMLD represents the last depths up to which $\Delta\rho$ is consistently small from the surface to the pycnocline, while the BMLD is the first depth after the pycnocline from which $\Delta\rho$ is consistently small up to the seabed (Fig. 2).
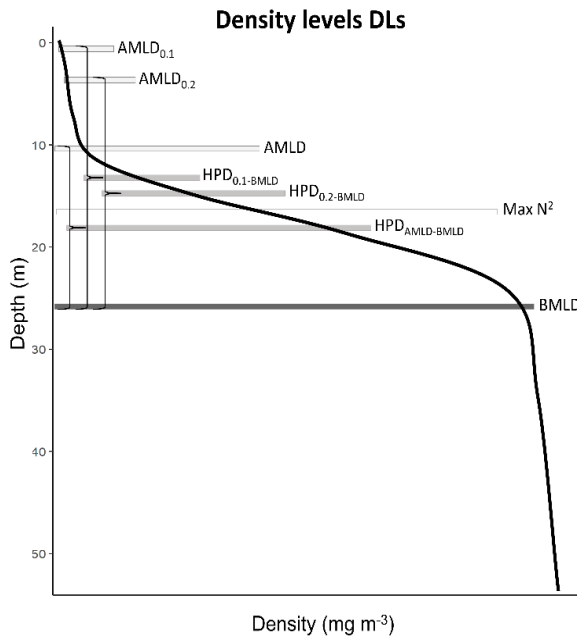
160   *Figure 2: The eight density levels (DLs) are reported for a generic density profile. The curly brackets define the halfway depths (HPDs) between AMLD's indicators (AMLD$_{0.1}$, AMLD$_{0.2}$, AMLD) and BMLD.*

Method to extract AMLD and BMLD

AMLD and BMLD have been identified developing an algorithm based on Chu and Fan (2011) framework to produce a method able to cope with various density profiles exhibiting a pycnocline (examples in Fig. A1 in Appendix A). The

165   algorithm's sequence identifies the depth with the largest density difference between a mixed and a stratified layer using i) an adaptation of the maximum angle method (Chu and Fan, 2011) and ii) a cluster analysis on the density difference at each observed depth ($\Delta\rho_z = |\rho_z - \rho_{z+1}|$). The method is designed to work with equal, high-resolution, intervals of density values (z) in the profiles. In order to distinguish AMLD from BMLD, their selection is achieved by splitting the number of observations throughout the profile into two distinct groups, *Split1* and *Split2* (Fig. 3), each one respectively

170   used to identify AMLD and BMLD. *Split1* includes the density values from the surface (z_1) to two measurement intervals (δ, here 1 m) above BMLD ($z_{BMLD} - 2\delta$); *Split2* extends from 2δ above the halfway depth in ρ range ($0.5\Delta\rho = ((\rho_{max} - \rho_{min})/2) - 2$) to the ninetieth portion of the profile from the surface to the seabed ($z_{0.9\Delta\rho} = 90\%$ of $\frac{n}{1}z$) (Fig. 3). For all depths between z_1 and $z_{0.9\Delta\rho}$, the angle φ has been measured at $z(x,y)$ (where x and y are density and depth) between two vectors (V1, V2) fitting a linear regression ($y \sim x$). Although Chu and Fan (2011) suggested to measure the tangent of

175   the angle between V1 and V2 (φ), we encountered some issues identifying BMLD in those profiles where density decreases below the pycnocline (Fig. A1d, Appendix A) and φ is bigger than 90 degrees. However, the exclusive use of the maximum angle method would have biased the selection due to local variation and instability conditions of the water column (Fig. A1b, c, e, f in Appendix A). Therefore, a K-Mean cluster analysis (Lloyd, 1982) was adopted in the algorithm to improve the selection of the pycnocline limits by classifying the density difference at depth ($\Delta\rho_z = |\rho_z - \rho_{z+1}|$) into

180   groups. The use of K-mean meets the assumption that $\Delta\rho_z$ values within a mixed layer would belong to a unique cluster. Adding the conditions controlling for a similar classification of $\Delta\rho_z$ at depths above AMLD and below BMLD resulted in decisive outcomes, correctly identifying the mixed layers within those density profiles having a pycnocline fractured in chunks with different or similar gradients. The algorithm was developed in R v3.6.3 (R Core Team, 2018) and it is

available as a function (*abmld.R*) to download from GitHub (https://github.com/azampollo/BMLD). A more detailed
description of the method is also reported in Supplementary Materials at the GitHub page.
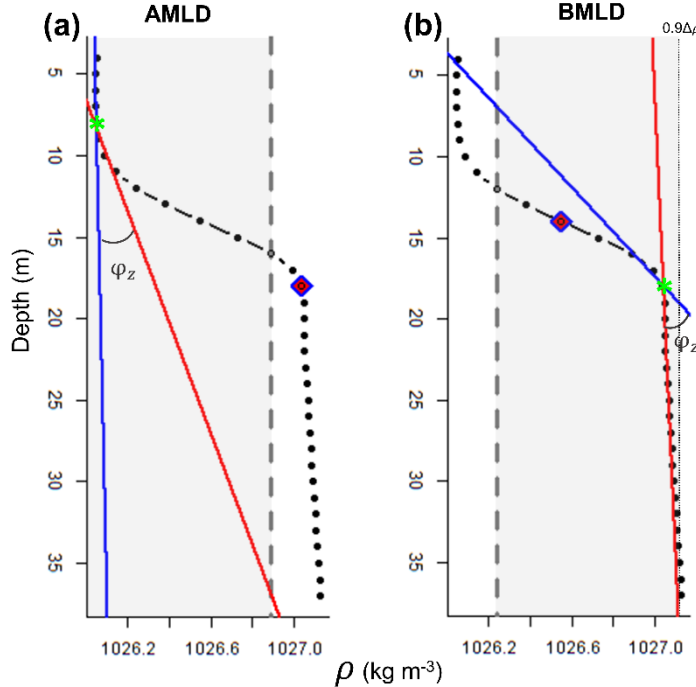
Figure 3: plots of a density profile reporting the attributes calculated by the algorithm: grey region includes the observations (black dots) used to identify AMLD and BMLD, which extends in (a) from the surface to 2δ before BMLD (purple rhombus), and in (b) from 2δ before the reference point (0.5Δρ, purple rhombus) to 0.9Δρ. The solid blue and red lines refer to the vectors V1 and V2 reporting the angle φ$_z$ used to identify AMLD and BMLD (green stars).

Performance of the algorithm

Following the assumptions described above, the algorithm failed to correctly identify AMLD and BMLD and classified the two limits of the pycnocline within it (examples in Fig. A1, Appendix A). The selection was considered to have failed when the AMLD and BMLD were selected ≥ 2 m (2 observations) above or below the mixed layer depth. Major errors in identifying AMLD (6.76% of the profiles) and BMLD (4.32%) occurred in density profiles with a high number of observations in the portion of the water column where mixed layer was transiting into the pycnocline, where φ$_z$ was similar amongst several observations and the cluster analysis was identifying observations at the end of the pycnocline as part of the mixed layer (e.g. Fig. A1 a-c, Appendix A). It is important to highlight the sensitivity of this method to Δρ at AMLD and BMLD (a large Δρ is preferred), and the sampling frequency at the transition between the pycnocline and the above and below mixed layers. The algorithm did not correctly identify AMLD in profiles without a surface mixed layer, and a shallow pycnocline that comprised two different gradients (Fig. A1c, Appendix A). In this case, the cluster analysis split Δρ into two groups, although they belong to the same pycnocline. Other errors were related to profiles having a pycnocline split into two parts by a thin mixed layer with height > 4 m (4 observations) (Fig. A1e, Appendix A). Overall, the identification of BMLD performed better than AMLD's, although it could not deal with profiles having less than 4 observations throughout the pycnocline (in this study thickness of the pycnocline < 3 m). This condition occurred due to the location of the *Split2* (which is necessary to distinguish BMLD's from AMLD's selection) i) at depths above AMLD (misidentifying AMLD as BMLD) or ii) too close to BMLD (missing enough observations to fit properly V1). The

algorithm always correctly selected BMLD in profiles that have a lower density observation below the BMLD (Fig. A1d, Appendix A).

2.3 Common methods identifying Density Levels (DLs)

Among the methods used to detect density levels in coastal and oceanic waters, three approaches were selected to define mixing and buoyancy features in the sampled profiles.

The AMLDs are typically defined as MLD in the literature and represent the depth at which the density exceeds a specific value (threshold method) (e.g. Kara et al., 2000). The threshold is typically selected among a range of values previously tested in the literature (from 0.0025 to 0.125 kg m^{-3}) (summarized in Thomson and Fine, 2003; Montégut et al., 2004; Lorbacher et al., 2006; Holte and Talley, 2009) and measured as the difference ($\Delta\rho_z = |\rho_z - \rho_{ref}|$) between a certain sampling depth (z) and a reference density value (ρ_{ref}), which can be the density at the surface, at 10 m depth, or a consecutive point (e.g. z-1). In this study, two density thresholds (0.01 and 0.02 kg m^{-3}) have been measured as the difference between two consecutive points in the profile ($\Delta\rho_z = |\rho_z - \rho_{z+1}|$) and named as AMLD$_{0.01}$ and AMLD$_{0.02}$. Since previous studies identified subsurface Chl-a in the proximity of the centre of the pycnocline (here called halfway pycnocline depth, HPD, Table 1), we investigated the relationship between CMd (depth of maximum Chl-a) and three different HPDs measured as the halfway depth between the base of the pycnocline (BMLD) and AMLD$_{0.01}$, AMLD$_{0.02}$ and adjusted AMLD, and named HPD$_{0.01-BMLD}$, HPD$_{0.02-BMLD}$, and HPD$_{AMLD-BMLD}$ (Fig. 2).

Moreover, several studies reported positive correlation between the maximum squared buoyancy frequency (Max N^2) and CMd at oceanic sites (e.g. Martin et al., 2010; Schofield et al., 2015; Carvalho et al., 2017; Courtois et al., 2017; Baetge et al., 2020) and shelf waters (Lips et al., 2010; Zhang et al., 2016). Therefore, the depth of Max N^2 has been selected from N^2 profiles computed by *gsw_Nsquared* function (*gsw* v1.0-5 package) in R v3.6.3 (R Core Team, 2018), following the most recent version of the Gibbs equation of state for seawater in TEOS-10 systems (Intergovernmental Oceanographic Commission, 2010). The magnitude of N^2 quantifies the stability of the water column and pinpoints the stratified layers where the energy required to exchange water parcels in the vertical direction is maximum (Boehrer and Schultze, 2009).

Table 1: Table of abbreviations used in the paper.

Abbreviation	Description
SCML	*Subsurface Chlorophyll-a maximum Layer*
Chl-a	*Chlorophyll-a (mg m^{-3})*
CMd	*Depth of maximum Chlorophyll-a (m)*
DL	General abbreviation for a *density layer* (e.g. AMLD, BMLD, HPD, or Max N^2) *(m)*
MLD	General expression for *Mixed layer depth (m)*
AMLD	*Above mixed layer depth,* or starting point of the pycnocline *(m)*
BMLD	*Below mixed layer depth*, or ending point of the pycnocline *(m)*
HPD	*Halfway pycnocline depth,* or centre of the pycnocline *(m)*
Max N^2	maximum squared buoyancy frequency (N^2) *(m)*

2.4 Subsurface Chlorophyll-a parameters

The depth of maximum Chl-a (CMd) was defined as the deepest maximum inflection point in the Chl-a profile standardized at 1 m sampling frequency (Carvalho et al., 2017; Zhao et al., 2019b), by using the adapted Chu and Fan (2011) method described in Sect 2.2. The CMd was selected throughout each vertical profile of Chl-a as the depth having the maximum angle (φ) between two vectors (V1 and V2). Details on the number of observations used to fit each vector are reported in Supplementary materials. The automated identification of CMd was checked manually with a visual inspection of each profile. The total amount of Chl-a were measured using trapezoidal integration (Walsby, 1997) throughout the water column (depth-integrated Chl-a) in R v3.6.3 (R Core Team, 2018).

2.5 Evaluating the association of density levels with subsurface Chl-a

The ecological relevance of each density level (DL) was evaluated by comparing their coincidence with the depth of maximum Chl-a (CMd) (e.g. CMd = BMLD) and their strength in predicting CMd. The coincidence and the prediction of CMds from density profiles return important understanding of the processes driving subsurface concentrations and identify a valuable proxy for modelling analyses and for controlling uncertainty in net primary production estimates.

In this study, we evaluated the coincidence of the CMd with eight investigated density levels ($AMLD_{0.01}$, $AMLD_{0.02}$, AMLD, BMLD, $HPD_{0.01-BMLD}$, $HPD_{0.02-BMLD}$, $HPD_{AMLD-BMLD}$, and Max N^2, Fig. 2) using Spearman's rank correlation coefficient (ρ_S) and a Major Axis (MA) line fitting, and the prediction of CMd from DL by performing a linear regression model (LM). The Spearman's coefficient (Eq. (1) in Table 2) assesses a monotonic linear relationship with values ranging between -1 and +1, which refer to a perfect negative or positive correlation between two variables. Besides the strength of the linear relationship defined by ρ_S, we focused on evaluating the linear relationship between CMd and each DL using 3 different linear models $y = \alpha + \beta x$: 1) alpha and beta estimated by linear regression ; 2) alpha and beta estimated by major axis line fitting; and 3) the one-to-one linear regression with alpha and beta fixed at 0 and 1 respectively. The one-to-one line hypothesizes that CMd and DL occur at the same depth. The MA is largely used to investigate how one variable scales against another by accounting for errors from both directions (x and y) and measuring the residuals perpendicular to the line (details in the review Warton et al., 2006). Therefore, the aim of MA is not to predict the y-variable, however evaluating the proximity of the coefficients of the estimated MA line (α and β) to the scenario in which DL equals CMd. The coincidence of each DL and CMd was summarized by reporting the α and β MA coefficients, which are hypothesized to be intercept ~ 0 and slope ~ 1 when CMd occurs at the same depth of the DL in question.

Since the identification of a proxy for subsurface Chl-a represents a useful tool for correctly assessing the abundance and the variations of primary production, we investigated the power of prediction of CMd from each DL by measuring the r-squared (R^2) from i) an ordinary least square to estimate parameters from the observations in a linear regression (Eq. (2) in Table 2), and ii) the one-to-one linear regression (which has been forced with the intercept through the origin and a slope equal to 1, Eq. (3) in Table 2). The formulae used to calculate the coefficient of determination R^2 for the one-to-one (R_0^2) and empirical (R_{em}^2) LMs are summarized in Eq. (2) and Eq. (3) in Table 2.

Table 2: Formulae for estimating the bivariate line-fitting. Spearman's rank correlation coefficient (ρ_S), coefficient of determination R^2 for testing the one-to-one linear regression (R_0^2) (e.g. CMd $\sim$ BMLD) and the empirical linear regression (R_{em}^2).

	Formula		Purpose
ρ_S	$\dfrac{\sigma_{xy}}{\sigma_x \sigma_y}$	(1)	Estimate the strength of the relationship between x and y

R_{em}^2	$1 - \dfrac{SS_{RES}}{SS_{TOT}} = 1 - \dfrac{\sum_{i=1}^{n}(y_i - \hat{y}_i)^2}{\sum_{i=1}^{n}(y_i - \bar{y})^2}$ (2)	Measure the variation in y that is explained by x in a LM
R_0^2	$1 - \dfrac{SS_{RES}}{SS_{TOT}} = 1 - \dfrac{\sum_{i=1}^{n}(y_i - x_i)^2}{\sum_{i=1}^{n}(y_i)^2}$ (3)	Measure the variation in y that is explained by x in a one-to-one LM

Notation: σ_{xy} is the covariance of x and y, σ_x and σ_y are standard deviations, n is the number of observations of x and y, y_i is DMC_i, $\bar{y}$ is the average of CMds, and x_i is the density layers related to CMd in each regression (e.g. CMd ~ BMLD). SS_{RES} is the residual sum of squares, SS_{TOT} is the total sum of squares.

In the empirical LM, R_{em}^2 was calculated using the typical formula with the residual sum of squares (SS_{RES}) as the square of the difference of y and $\hat{y}$ (estimated y from the model) (Eq. 2)). In the one-to-one LM, the SS_{RES} in R_0^2 was adapted by replacing $\hat{y}$ with x (Eq. (3)), since the values of x and y are assumed to be equal in the one-to-one line regression and the difference between them should be zero. The two R^2 differ also for the denominator SS_{TOT}, which is the sum of squares about the average of the explanatory variable in R_{em}^2 and the sum of squares of the CMd values since in R_0^2 the value of CMd and DL equals.

Since the SS_{TOT} adopted in the two formulae is different, the proportion of explained CMds' variance by each DL can be compared only within each linear regression rather than across the one-to-one and empirical regressions. Therefore, the power of prediction among DLs was discussed in within each type of LM.

3. Results

The presented algorithm identifying for AMLD and BMLD was applied to 1273 profiles exhibiting a pycnocline. The associations of the density levels (AMLD$_{0.01}$, AMLD$_{0.02}$, AMLD, HPD$_{0.01\text{-BMLD}}$, HPD$_{0.02\text{-BMLD}}$, HPD$_{\text{AMLD-BMLD}}$, BMLD and Max N^2) with CMds and the vertical distribution of Chl-a are described in Sect 3.1 and 3.2.

3.1 Vertical distribution of CMd and density levels

The depth of Chl-a maximum (CMd) was compared to eight different levels of the density profile that are summarized in surface mixed layer depth (AMLD$_{0.01}$, AMLD$_{0.02}$, AMLD), below mixed layer depth (BMLD), the centre of the pycnocline (HPD$_{0.01\text{-BMLD}}$, HPD$_{0.02\text{-BMLD}}$, HPD$_{\text{AMLD-BMLD}}$) and the depth of maximum buoyancy frequency squared (Max N^2) to evaluate i) the strength of a positive linear relationship between each DL and CMd, and ii) the prediction of CMd from each DL.

The observations carried out in the FoF and Tay region confirmed the subsurface presence of maxima Chl-a between April and August, with CMds distributing on average ($\pm$ standard deviation) at 19.29 ± 6.56 m. All the indicator classifying the surface mixed layer (AMLD$_{0.01}$, AMLD$_{0.02}$ and AMLD) distributed generally shallower than CMds (Fig. 4 a-c, Table 3) with a rare coincidence of their vertical distribution (from 0.39% to 1.73% of the profiles, Table 3). In particular, the thresholds' methods used to identify AMLD (0.01 and 0.02 mg m^{-3}) exhibited the lowest Spearman correlation amongst all DLs, having almost a zero correlation to CMds (ρ_S = -0.01 and 0.08 for AMLD$_{0.01}$ and AMLD$_{0.02}$, Table 3) and a limited contribution to define CMd's variability in empirical linear regressions (R_{em}^2 = 0.00 and 0.01, Table 3). The Major Axis analysis measured intercepts and slopes in AMLD$_{0.01}$ and AMLD$_{0.02}$ almost perpendicular to the y-axis due to the strong presence of CMds in deep waters. Although a clear subsurface aggregation of Chl-a maxima occurs below the surface mixed layer (Fig. 4c), the AMLD identified by the algorithm correlated better to CMd than AMLD$_{0.01}$ and AMLD$_{0.02}$, with a positive linear relationship between the two variables and a greater explained variance of CMd by

the one-to-one and empirical linear regressions (Table 3). The coefficients measured by MA for AMLD (Table 3) reported a positive correlation of CMds, representing a gradual deepening of CMd with the pycnocline.

Max N^2 is the density level performing least well after AMLDs in predicting CMds, although it showed the highest percentage of coincidence with CMds (13.51% of the profiles, Table 3). Similar to AMLDs, CMds have been recorded in 64.96% of the profiles at layers deeper than Max N^2, indicating that Chl-a maxima area located in waters below surface mixing, at stratified regions within the pycnocline.

Overall, the centre of the pycnocline (HPDs) performed better than AMLD and Max N^2, distributing closer to CMds. $HPD_{AMLD-BMLD}$ reported the highest correlation to CMds ($\rho_S = 0.56$), and the highest explained CMd's variance from the one-to-one ($R_0^2 = 0.90$) and empirical ($R_{em}^2 = 0.31$) linear regressions (Table 3). The location of CMds is highly related to $HPD_{AMLD-BMLD}$, although only 4.63% of the profiles presented CMds and $HPD_{AMLD-BMLD}$ at the same depth (Table 3). Many profiles exhibited CMd deeper than $HPD_{AMLD-BMLD}$ (78.69%), of which 81.53% distributed CMds above BMLD (hence, between $HPD_{AMLD-BMLD}$ and BMLD). $HPD_{0.01-BMLD}$, $HPD_{0.02-BMLD}$ less related to CMds in Spearman's correlation, MA, one-to-one and empirical linear regressions than the $HPD_{AMLD-BMLD}$ (Table 3).

The below mixed layer depth, BMLD, exhibited a reverse condition compared to the other density levels by encompassing 78.32% of CMds in waters above it (Table 3). BMLDs is the second variable after $HPD_{AMLD-BMLD}$ with the highest correlation to CMds ($\rho_S = 0.55$). It is distributed at the same depth of CMds in 7.86% of the profiles and linearly predicted the location of maxima Chl-a in both one-to-one and empirical linear regressions (Table 3). BMLD exhibited MA coefficients ($\alpha = 0.60$ and $\beta = 0.82$) close to the hypothesized one-to-one fitting-line ($\alpha = 0$ and $\beta = 1$), indicating a good approximation of CMds at the base of the pycnocline. Moreover, CMds distributed on average at 2.74 ± 5.21 m above BMLD, with a maximum distance above it equals to 22 m, and 27 m below it.

The overall distribution of CMds is discernible mainly (> 95.84% of profiles) below the surface mixed layers (AMLDs' indicators), within the deepest half of the pycnocline (between $HPD_{AMLD-BMLD}$ and BMLD) and it is bounded for 78.32% of the observations above the BMLD. Although CMds generally reflect the region with the highest concentration of Chl-a throughout the water column, the vertical distribution of Chl-a can vary in the proximity of CMds and accumulate mainly above or below it. Hence, the ecological relevance of the density levels has been investigated in comparison with the vertical distribution of Chl-a (Sect. 3.3).
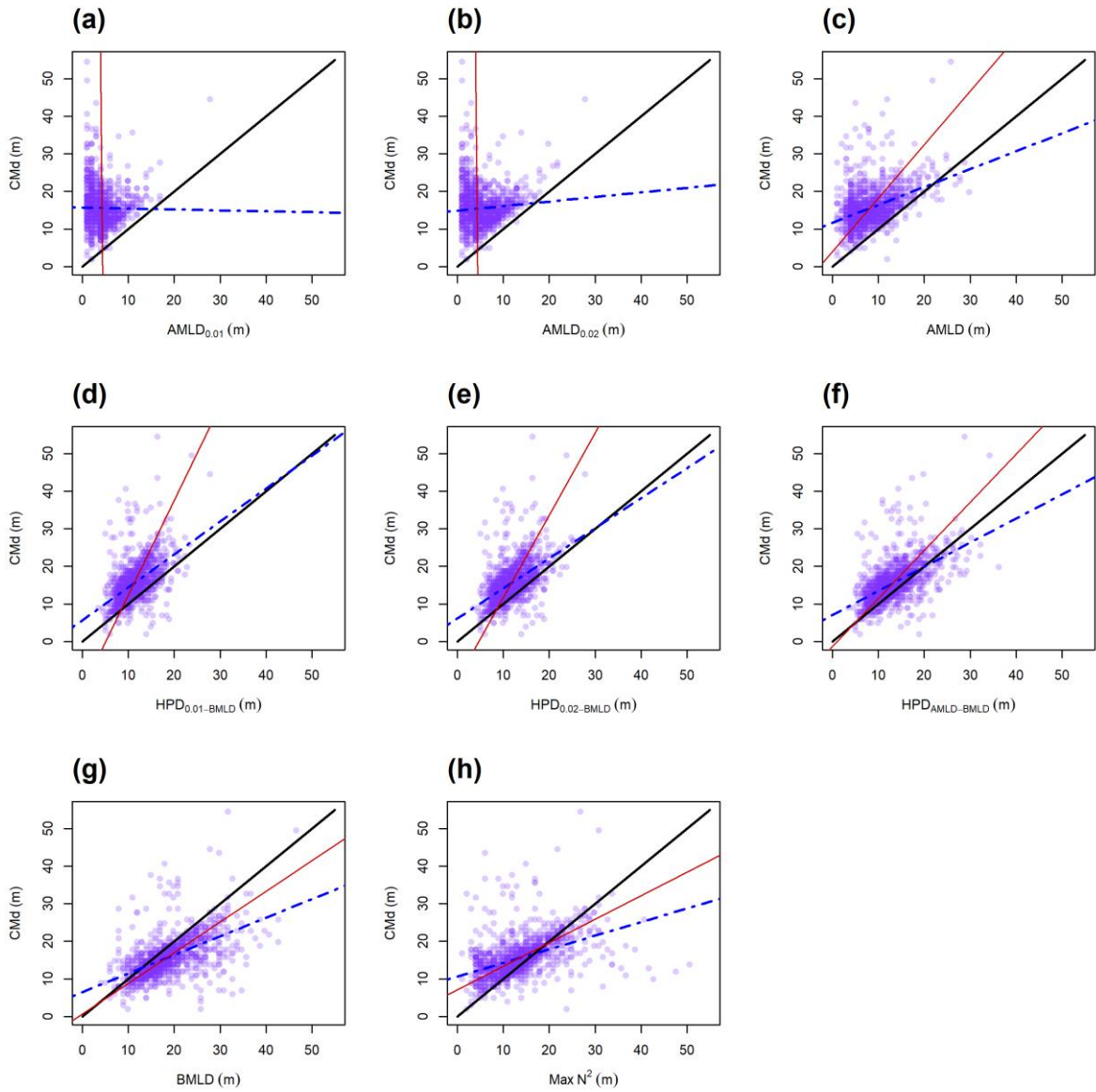
Figure 4: Scatterplots of CMd and the eight DLs (a-h). The lines refer to the one-to-one linear regression (LM) (solid black), the Major Axis analysis (MA) (solid red), the empirical LM measured from the observations (CMd ~ DL) (dot-dashed blue).

Table 3: Statistical parameters and percentage of profiles having CMds above (>), at the same depth (=), or below (<) each DL.

DL	ρ_S	α	β	R_0^2	R_{em}^2	CMd > DL	CMd = DL	CMd < DL
$AMLD_{0.01}$	- 0.01	543.35	-124.26	0.40	0.00	99.53	0.39	0.08
$AMLD_{0.02}$	0.08	-43.72	11.35	0.47	0.01	99.45	0.31	0.24
AMLD	0.41	4.01	1.42	0.69	0.17	95.84	1.73	2.44
$HPD_{0.01-BMLD}$	0.52	-12.81	2.52	0.86	0.27	90.18	1.81	8.01
$HPD_{0.02-BMLD}$	0.52	-10.20	2.19	0.87	0.27	86.41	3.77	9.82
$HPD_{AMLD-BMLD}$	0.56	1.31	1.28	0.90	0.31	74.86	4.63	20.50
BMLD	0.55	0.60	0.82	0.87	0.31	13.83	7.86	78.32

335

Max N^2	0.45	7.06	0.63	0.84	0.20	64.96	13.51	21.52

3.2 Chl-a vertical distribution in relation to density levels

340 Since hydrodynamic and biological conditions generating resuspension, passive drift, and mortality (i.e. zooplankton grazing in stratified waters) shape Chl-a differently throughout the water column, the amount of Chl-a was measured above and below each density levels regardless the vertical distribution of CMd.

The depth-integrated Chl-a was standardized by the number of observations above and below four DLs (AMLD, $HPD_{AMLD-BMLD}$, BMLD and Max N^2). AMLD and $HPD_{AMLD-BMLD}$ were selected amongst the density levels to represent 345 the surface mixed layer and the centre of pycnoclines because of their better correlation to CMd (see Sect. 3.1). The amount of Chl-a at each meter depth (mg m^{-1}) above and below the four density levels is reported in Table 4 and Figure 5.

Table 4: Values of depth-integrated Chl-a (mg) standardized by its range of vertical distribution (m) (Total Chl-a biomass (mg)/depths (m)) above and below the four density layers. These values are also reported in Figure 5.

DL	Standardized depth-integrated Chl-a above DL (mg m^{-1})	Standardized depth-integrated Chl-a below DL (mg m^{-1})
AMLD	172.97	971.12
$HPD_{AMLD-BMLD}$	366.07	859.27
BMLD	615.92	658.72
Max N^2	372.90	848.14

350
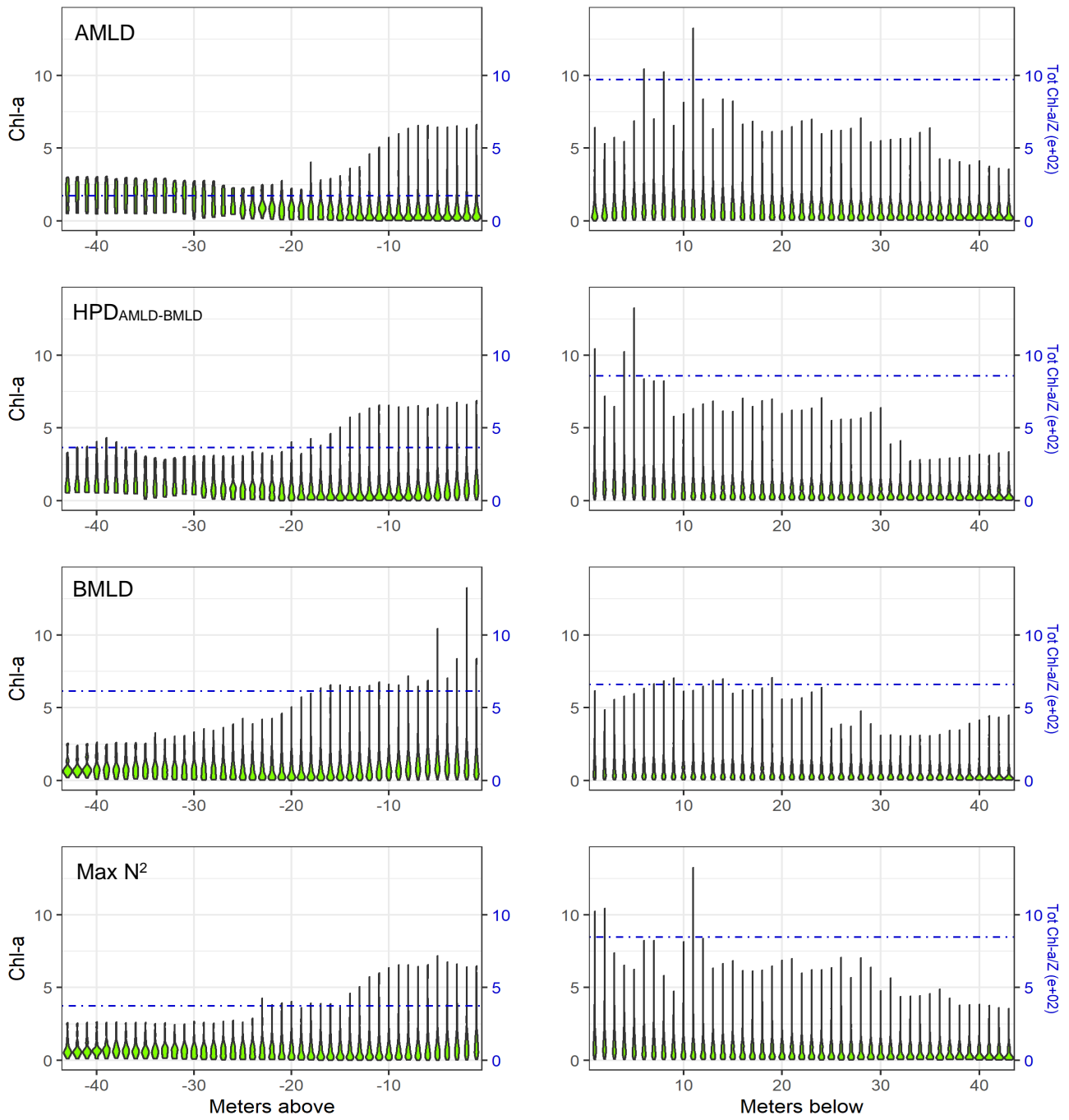
Figure 5: Violin plot of Chl-a (mg) at each meter above and below the four density levels (AMLD, HPD$_{AMLD-BMLD}$, BMLD and Max N^2) for the whole dataset. The dot-dashed blue lines represent the depth-integrated Chl-a measured as the total amount of Chl-a (mg) divided by the number of depths (z) within each portion of the water column (above and below DLs) (values are reported in Table 4).

Following the results in Sect. 3.1, a large portion of Chl-a was measured at depths below AMLD, HPD$_{AMLD-BMLD}$ and Max N^2 (Table 4), where the depth of Chl-a maximum also occurred. From the seabed to HPD$_{AMLD-BMLD}$ and Max N^2, the amount of Chl-a was three times the Chl-a from these DLs to the surface. A reverse condition occurred for Chl-a distributing above and below BMLDs: the standardized depth-integrated Chl-a is higher above BMLDs, although the amount of Chl-a in the deepest layers (below the pycnocline) is still comparable (the difference between Chl-a from the surface to BMLD and from BMLD to seabed is 42.80 mg m^{-1}) (Table 4).

It is therefore sensible to infer the distribution of CMds, and the largest portion of Chl-a at depths enclosed within the stratified region (AMLD – BMLD), especially in the second half of the pycnocline (HPD$_{AMLD-BMLD}$ – BMLD). At the same time, a noticeable amount of Chl-a still distributes below the pycnocline (BMLD).

4. Discussion

In stratified waters, the vertical distribution of Chl-a is regulated by the balance of stratification and mixing rates across different hydrodynamic regimes over time (Leeuwen et al., 2015). The combination of static, dynamic and biological factors (e.g. grazing, Benoit-Bird *et al.*, 2013) induces phytoplankton communities to adapt their vertical distribution at small scales (< 1 km, Scott et al., 2010; Sharples et al., 2013). Identifying a proxy for subsurface concentrations of Chl-a is essential to investigate the impacts of physical changes due to large scale factors (e.g., stratification strength, sea water increase, or turbulence increase downstream wind turbine foundations). To date several studies have identified the mixed layer between the sea surface and the pycnocline as a valuable tool to assess changes in phytoplankton abundance and phenology over time; here we propose a tool to identify the vertical limits of the pycnocline and indicate the base of the pycnocline (BMLD) as a variable tightly influencing the vertical distribution of Chl-a and likely to affect abundance and phenology.

4.1 Ecological relevance of AMLD and Max N^2 in defining CMds

Oceanic sites exhibit phytoplankton blooms within the upper mixed layer (e.g. Behrenfeld, 2010; Costa et al., 2020; Somavilla et al., 2017) to coincide with AMLDs' vertical fluctuations due to e.g. windstorm events deepening the pycnocline into nutrient-enriched waters (Detoni et al., 2015; Carranza et al., 2018; Höfer et al., 2019; Montes-Hugo et al., 2009). In this study, all the investigated surface mixed layers' indicators (AMLD$_{0.01}$, AMLD$_{0.02}$ and AMLD) weakly predicted CMd. The algorithm used in this study has identified AMLD to have an overall higher performance in predicting the location of CMds than the thresholds' methods and maximum squared buoyancy frequency (Max N^2). Since AMLD has been largely considered as a central variable for understanding phytoplankton dynamics (Sverdrup, 1953), it has been investigated in relation to climate change to infer possible significant changes in the amount, spatial distribution and phenology of oceanic primary production (Boyd et al., 2015; Montes-Hugo et al., 2009; Somavilla et al., 2017; Prend et al., 2019; Richardson and Bendtsen, 2019; Schmidt et al., 2020). However, the effect of climate change on AMLD and primary production is still an unsolved question (Lozier et al., 2011; Somavilla et al., 2017). The unclear effects of climate change on AMLD and primary production might be related to i) the type of data used to measure variations in Chl-a, e.g. satellites' observations at the sea surface and their uncertainty related to subsurface Chl-a (Baldry et al., 2020; Erickson et al., 2016; Lee et al., 2015), and ii) the exclusive investigation of the effects of surface mixing processes on primary production (e.g. temperature, wind-induced mixing) by neglecting deep processes that are responsible for the pycnocline's stability (Dave and Lozier, 2015, 2013; Lozier et al., 2011; Somavilla et al., 2017). The AMLD is informative for surface concentrations, but it may not be biologically relevant for subsurface Chl-a that are maintained at the pycnocline by deep turbulent mixing. The need for a much more detailed understanding of the linkage between subsurface Chl-a, pycnocline characteristics and deep turbulent processes is therefore a key subject, especially in highly productive but spatially heterogeneous areas such as shelf waters and shallow seas.

In the FoF and Tay region, Max N^2 exhibited higher percentages of coincidence with CMds (13.51% of 1273 profiles) than other DLs (Table 3). The depth of Max N^2 is a less turbulent region where the energy to exchange parcels in the vertical is maximum (Boehrer and Schultze, 2009), and it is frequently used to identify the upper mixed layer depth (e.g. Carvalho et al., 2017). The location of CMds at Max N^2 might reflect the distribution of phytoplankton within a less

turbulent region where nutrient particles, which have been resuspended by mixing, can persist for longer time periods. The mild turbulent layer at Max N^2 would therefore represent a hot spot of nutrients reached by resuspended phytoplankton cells, while strong mixing processes still undergoing above and/or below it, or diluted gradients of phytoplankton and nutrients throughout the water column, would avoid the creation of highly productive subsurface patches. However, the amount of standardized depth-integrated Chl-a below Max N^2 is almost three times higher than above it (Table 4 and Fig. 5) suggesting that Max N^2 is a layer of suitable conditions for phytoplankton to grow, but it lacks informing where most of the Chl-a vertically distribute. Although the depth of Max N^2 appeared to inform better the exact location of CMds, BMLD exhibited a clear pattern by distributing below CMd in 78.32% of the profiles and representing the deepest limit up to which CMds distributed. Overall, the linear correlation (ρ_S), the MA coefficients and the one-to-one linear regression R_0^2 described a low association of CMds with Max N^2 compared to HPDs' indicators and BMLD, and hence the use of Max N^2 to locate subsurface Chl-a patches in summertime shelf waters may lead to underestimate the amount of Chl-a in the whole water column.

4.2 Vertical distribution of Chl-a and BMLD

The observations carried out in the FoF and Tay region confirmed the subsurface presence of maxima Chl-a between April and August. A recent study in the German Bight described CMds located mainly at the centre of the pycnocline and the overall amount of Chl-a at depths distinctly lower than the surface mixed layers (Zhao et al., 2019a). The location of CMd at the pycnocline is regulated over time by upward nutrient-enriched fluxes entering the pycnocline from deep waters (Pingree et al., 1982; Rosenberg et al., 1990). In the Skagerrak strait between Denmark and Norway, deep SCMLs were recorded at a nutricline (rate of change in nitrate and phosphate) located below the base of a shallow pycnocline (< 15 m) (Bjørnsen et al., 1993). The low concentration of CMds below BMLD might reflect a limited erosion of Chl-a by mixing (Zhao et al., 2019a) and grazing (Benoit-Bird et al., 2013). The physical factors developing subsurface Chl-a are defined by mixing processes below the pycnocline that provides an indispensable upward flux of nutrients in the euphotic zone, where e.g. dinoflagellates are able to compete successfully in slightly turbulent conditions (< 0.1 mm s^{-1}) (Ross and Sharples, 2007). Therefore, the erosion as well as the resuspension of sinking phytoplankton cells and nutrients can maintain the proximity of CMds at BMLDs setting the location of the nutricline at the base of the pycnocline. It is also noticeable that a large amount of diluted Chl-a in deep waters (51.67% of depth-integrated Chl-a below BMLD) might be crucial in maintaining primary production at the subsurface over the summer, since deep mixing processes eroding and sustaining Chl-a at BMLD would contribute also to reducing the overlap between SCMLs and predators (Behrenfeld, 2010).

Overall, the deep distribution of CMds, and most of the depth-integrated Chl-a, in the proximity of the centre and the base of the pycnocline suggests the maintenance of subsurface Chl-a within shelf waters through the regulation of nutrient supply by waters below the pycnocline and makes this linkage responsive to variations in deep physical processes.

4.3 Using BMLD to investigate impacts on primary production

The marine photosynthetic activity represents an essential biological pump of carbon sequestration (Boyd et al., 2015), whose extent is often invalidated by the exclusion of subsurface Chl-a of up to 10%-40% (Sharples et al., 2001). The correct measurement of primary production throughout the whole water column is essential to address which factors affect absorbing atmospheric carbon dioxide in the marine environment. Recent studies reported a decrease of Chl-a biomass (Capuzzo et al., 2018; Schmidt et al., 2020) and a temporal shift of phytoplankton bloom (Silva et al., 2021) due to significant changes in the surface MLD. The Northeast Atlantic shelves experienced a summertime reduction of Chl-a in

the last 60 years leading to significant impacts on the food web, caused by an intensified stratification of the water column that maintains nutrient fluxes in deep waters (Capuzzo et al., 2018; Schmidt et al., 2020). Prolonged stratified conditions were reported to define deeper concentrated patches of Chl-a (Somavilla et al., 2017; Scott et al., 2010), where phytoplankton stabilize at deep low-turbulence layers (Bopp et al., 2013) having still sufficient light to photosynthesize and set the nitracline position. The starvation of nutrients at surface force phytoplankton to re-distribute in the water column (e.g. Bindoff et al., 2019; Boyd et al., 2015; Schmidt et al., 2020) in deeper nutrient-enriched waters within the euphotic zone. Hence, the location of CMds in the proximity of the deepest portion of the pycnocline, between $HPD_{AMLD\text{-}BMLD}$ and BMLD, (78.32% of the profiles) is not surprising during summer in the Firth of Forth and Tay regions. Although a consistent portion of depth-integrated Chl-a is reported below pycnocline, the vertical distribution of BMLD resulted in setting the position of subsurface productive patches in stratified waters, representing an important indicator of the vertical distribution of phytoplankton in shelf waters.

The effects of an intensified stratification on primary production in the continental shelf waters are still entangled and suggest an overall deepening of subsurface Chl-a, which is likely to delineate a knock-on effect on redistributing most of the higher trophic levels (e.g., zooplankton, fish) and affect the foraging success of highly adapted species. However, the deepening of productive patches is difficult to examine over large spatial scales, and remote sensing methods often lack reliability for subsurface data. The role of climate change in increasing stratification are likely to affect the distribution of BMLD and the upward fluxes, which may either redistribute food patches at major depths together with the deepening of BMLD and causing an overall reduction of primary production or shifts of community compositions.

It is hence reasonable to notice that the potential effects on primary production involves both surface and deep (below the pycnocline) processes, especially where multiple local changes (i.e. wind turbine foundations changing levels of mixing) repeated over large spatial areas (i.e. the North Sea) have an effect at different scales (van der Molen et al., 2014; De Dominicis et al., 2018; Carpenter et al., 2016). The upcoming interest of the offshore renewable sector in building offshore wind farms (OWFs) in the FoF and Tay region (www.marine.gov.scot) rises the need of drafting reliable environmental impact assessments able to identify key variables for estimating the effects in a holistic way. The consequences of offshore wind farms are likely to be related to bathymetry and mixing budgets, by affecting the stratification rate differently across several bathymetries. The vertical distribution of CMds at BMLDs appeared to be correlated to the bathymetry by exhibiting CMds closer to BMLDs at water depths comprised from, approximately, 40 to 70 m, CMds deeper than BMLD mainly in shallow waters < 60 m, and CMds above BMLD towards deeper waters up to 100 m (Fig. A3 in Appendix A). Previous studies identified a similar pattern in shallow waters where CMds were mainly recorded at or below the base of the pycnocline (Barth et al., 1998; Durán-Campos et al., 2019; Holligan et al., 1984; Zhao et al., 2019a). Although stratification is reported to intensify in shelf waters with climate change, the increase in turbulence downstream wind farms may counteract the local stratification (Carpenter et al., 2016; Schulien et al., 2017; Schultze et al., 2020) and affect the temporal and spatial distribution of Chl-a. Since the variation in stratification is a useful tool to address possible impacts on primary production, using BMLD is likely to be more efficient in predicting changes in the vertical distribution of Chl-a and its possible consequences. The deepening of BMLD within or even below the euphotic zone may lead Chl-a to decrease across shelf seas since phytoplanktonic cells would buoyance at deeper and darker depths. Hence, the use of AMLD to investigate physical alteration of climate change and man-made structures should be integrated with the use of BMLD and the understanding of physical processes at depth, together with changes in seabed temperature, and the slow down or increase of upward fluxes.

5. Conclusion

Chl-a vertical distribution gives important information about the state of development of the phytoplankton community, which is associated with mixed and stratified layers. The mixing processes above and below the pycnocline can have very different influences on Chl-a vertical distribution, dictating the concentration at subsurface patches that can distribute close to, above, or below the pycnocline.

Although the association of phytoplankton with AMLD has been largely described at large spatial scales within oceanic habitats, the presented study shows a weak linkage between AMLD and CMd in shelf waters, at a very high vertical resolution (1 m), compared to HPDs' indicators or BMLD, which has led to hypothesize a stricter association of summertime subsurface Chl-a with the bottom-half of the pycnocline. Therefore deep mixing processes, such as tidal currents in the North Sea, play a role in regulating summertime subsurface primary production and may regulate their distribution at BMLDs in stratified conditions. Considering the described associations of subsurface Chl-a with BMLD, it is evident how this variable can play a role in the assessment of productivity, since the deep mixing processes are equally (or more) relevant than the surface process in determining a shift of primary production at local or large scales. This association therefore advocates the investigation of the effect of anomaly-inducing processes occurring at and below the pycnocline (e.g. deep sea temperature, deep salinity, turbulence and physical processes at the BMLD), which are likely to influence primary production and the whole ecosystem dynamics within shelf seas (Trifonova et al., 2021). Understanding mechanisms affecting primary production at fine scales is very important to investigate as we are moving rapidly towards the deployment of hundreds GW in the wind energy sector from worldwide shallow seas (Gielen et al., 2019). BMLD is proposed as an ecological relevant variable for further oceanographic investigations in shelf waters, and the proposed approach is a valuable tool to extrapolate this variable from *in situ* vertical samples.

Appendix A
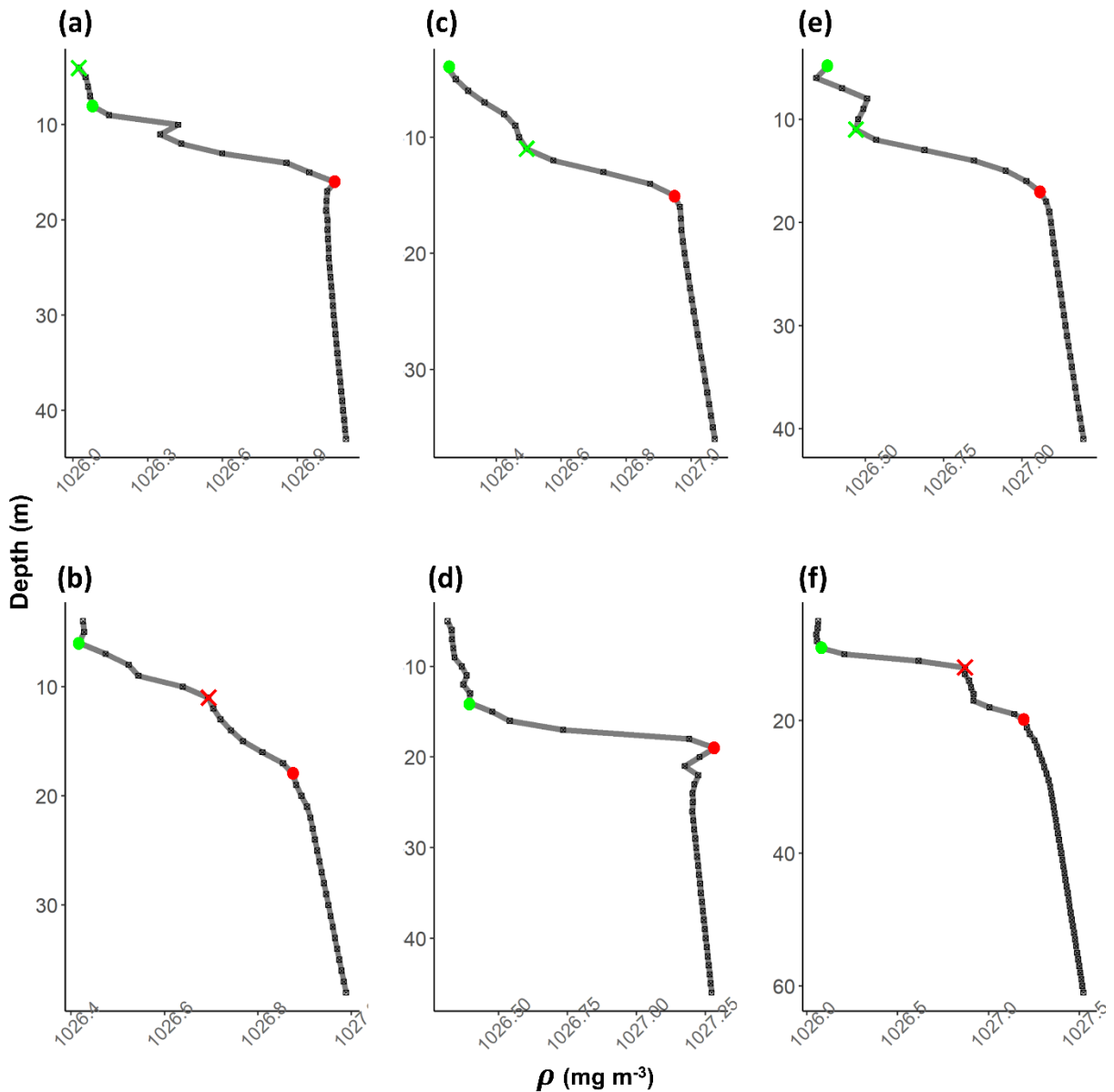
Figure A1: examples of density profiles (grey line) (a-f). The black squares are the values at 1 m resolution. Red dots refer to BMLD, green dots to AMLD. Crosses refer to misidentified AMLD (in green) and BMLD (in red) that needed to be manually corrected.

505
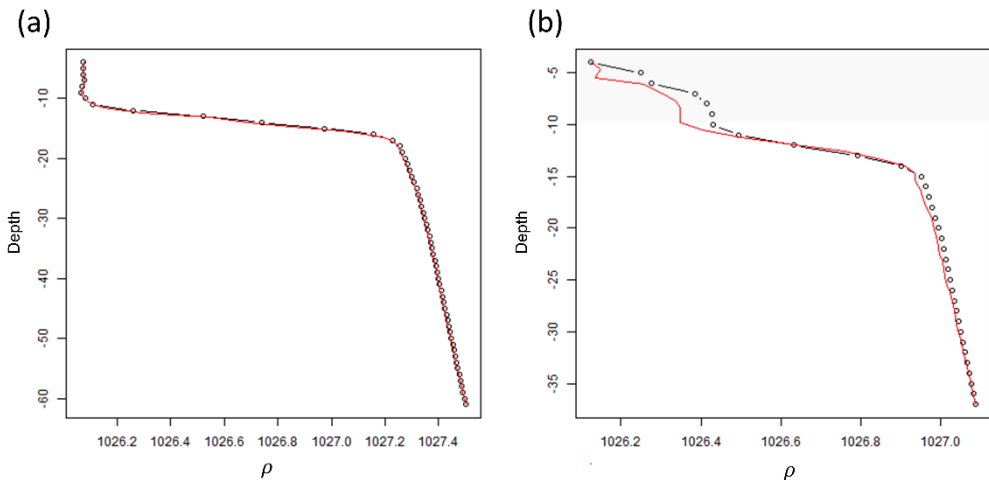
Figure A2: two density profiles whose observations were standardized at equals 1 m depths using generalized additive model (GAM). (a) reports a density profile (black dotted line) where GAM correctly fitted (red solid line) the vertical distribution. (b) reports a density profile where GAM wrongly fitted the upper portion of the profile (grey polygon area) and, hence, required a manual correction of the values.
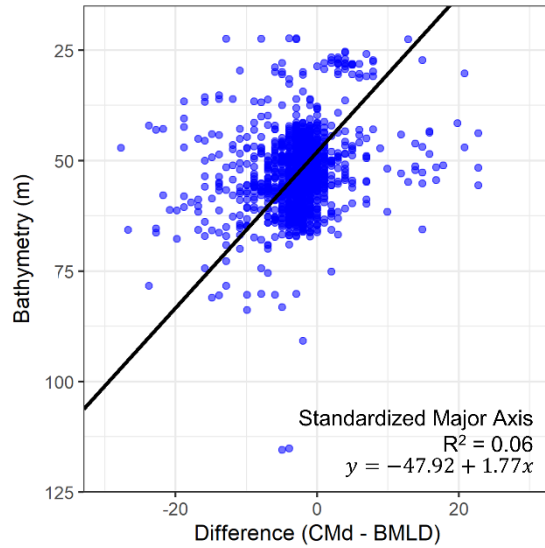
Figure A3: scatterplot of the difference between CMd and BMLD against the bathymetry at which each profile was sampled. The solid black line reports a Standardized Major Axis analysis, whose equation and R squared values are reported.

Author contribution

Arianna Zampollo contributed to the conceptualization of the study, formal analyses, methodology on AMLD and BMLD, writing of the original draft, and software use; Thomas Cornulier contributed to the conceptualization and supervision of the statistical method, writing of the original draft, methodology and visualization of the results; Rory O'Hara Murray contributed on the data curation, writing of the original draft, supervision, visualization and validation;

Jacqueline F. Tweddle contributed to the conceptualization and the supervision of the study; James Dunning contributed to the methodology of the AMLD and BMLD algorithm; Beth Scott contributed to the conceptualization of the analyses, writing of the original draft, supervision, funding acquisition, resources and data curation.

Code availability

525 The code for the AMLD and BMLD algorithm are available at https://github.com/azampollo/BMLD

Data availability

Data are available upon request and agreement with the co-authors.

Competing interests

The authors declare that they have no conflict of interest.

530 **Acknowledgment**

The authors thank the founding MarCRF, the Marine Collaboration Research Forum jointly sponsored by the University of Aberdeen and Marine Scotland Science, and Marine Scotland Science to provide a portion of the data.

References

Baetge, N., Graff, J. R., Behrenfeld, M. J., and Carlson, C. A.: Net Community Production, Dissolved Organic
535 Carbon Accumulation, and Vertical Export in the Western North Atlantic, Front. Mar. Sci., 7, 227, https://doi.org/10.3389/fmars.2020.00227, 2020.

Baldry, K., Strutton, P. G., Hill, N. A., and Boyd, P. W.: Subsurface Chlorophyll-a Maxima in the Southern Ocean, Front. Mar. Sci., 7, 671, https://doi.org/10.3389/fmars.2020.00671, 2020.

Banse, K.: Clouds, deep chlorophyll maxima and the nutrient supply to the mixed layer of stratified water
540 bodies, J. Plankton Res., 9, 1031–1036, https://doi.org/10.1093/plankt/9.5.1031, 1987.

Barth, J. A., Bogucki, D., Pierce, S. D., and Kosro, P. M.: Secondary circulation associated with a shelfbreak front, Geophys. Res. Lett., 25, 2761–2764, https://doi.org/10.1029/98GL02104, 1998.

Behrenfeld, M. J.: Abandoning Sverdrup's Critical Depth Hypothesis on phytoplankton blooms, Ecology, 91, 977–989, https://doi.org/10.1890/09-1207.1, 2010.

545 Benoit-Bird, K. J., Shroyer, E. L., and McManus, M. A.: A critical scale in plankton aggregations across coastal ecosystems: CRITICAL SCALE IN PLANKTON AGGREGATIONS, Geophys. Res. Lett., 40, 3968–3974, https://doi.org/10.1002/grl.50747, 2013.

Bindoff, N. L., Cheung, W. W. L., Kairo, J. G., Arístegui, J., Guinder, V. A., Hallberg, R., Hilmi, N., Jiao, N., O'Donoghue, S., Suga, T., Acar, S., Alava, J. J., Allison, E., Arbic, B., Bambridge, T., Boyd, P. W., Bruggeman,
550 J., Butenschön, M., Chávez, F. P., Cheng, L., Cinar, M., Costa, D., Defeo, O., Djoundourian, S., Domingues, C., Eddy, T., Endres, S., Fox, A., Free, C., Frölicher, T., Gattuso, J.-P., Gerber, G., Hallegraef, G., Harrison, M., Hennige, S., Hindell, M., Hogg, A., Ito, T., Kenny, T.-A., Kroeker, K., Kwiatkowski, L., Lam, V. W. Y., Laüfkotter, C., LeBillon, P., Bris, N. L., Lotze, H., MacKinnon, J., de Marffy-Mantuano, A., Martel, P., Molinos, J. G., Moseman-Valtierra, S., Motau, A., Mulsow, S., Mutombo, K., Oyinlola, M., Poloczanska, E. S., Pascal,
555 N., Philip, M., Purkey, S., Rathore, S., Rebelo, X., Reygondeau, G., Rice, J., Richardson, A., Riebesell, U., Roach, C., Rocklöv, J., Roberts, M., Sloyan, B., Smith, M., Shurety, A., Wabnitz, C., and Whalen, C.: Changing Ocean, Marine Ecosystems, and Dependent Communities, Mar. Ecosyst., 142, n.d.

Bjørnsen, P., Kaas, H., Kaas, H., Nielsen, T., Olesen, M., and Richardson, K.: Dynamics of a subsurface phytoplankton maximum in the Skagerrak, Mar. Ecol. Prog. Ser., 95, 279–294, https://doi.org/10.3354/meps095279, 1993.

560

Boehrer, B. and Schultze, M.: Density Stratification and Stability, in: Encyclopedia of Inland Waters, edited by: Likens, G. E., Academic Press, Oxford, 583–593, https://doi.org/10.1016/B978-012370626-3.00077-6, 2009.

Bonaduce, A., Staneva, J., Behrens, A., Bidlot, J.-R., and Wilcke, R. A. I.: Wave Climate Change in the North Sea and Baltic Sea, J. Mar. Sci. Eng., 7, 166, https://doi.org/10.3390/jmse7060166, 2019.

565

Bopp, L., Resplandy, L., Orr, J. C., Doney, S. C., Dunne, J. P., Gehlen, M., Halloran, P., Heinze, C., Ilyina, T., Séférian, R., Tjiputra, J., and Vichi, M.: Multiple stressors of ocean ecosystems in the 21st century: projections with CMIP5 models, Biogeosciences, 10, 6225–6245, https://doi.org/10.5194/bg-10-6225-2013, 2013.

570 Boyd, P. W., Lennartz, S. T., Glover, D. M., and Doney, S. C.: Biological ramifications of climate-change-mediated oceanic multi-stressors, Nat. Clim. Change, 5, 71–79, https://doi.org/10.1038/nclimate2441, 2015.

Brown, Z. W., Lowry, K. E., Palmer, M. A., van Dijken, G. L., Mills, M. M., Pickart, R. S., and Arrigo, K. R.: Characterizing the subsurface chlorophyll a maximum in the Chukchi Sea and Canada Basin, Deep Sea Res.
575 Part II Top. Stud. Oceanogr., 118, 88–104, https://doi.org/10.1016/j.dsr2.2015.02.010, 2015.

Capuzzo, E., Lynam, C. P., Barry, J., Stephens, D., Forster, R. M., Greenwood, N., McQuatters-Gollop, A., Silva, T., Leeuwen, S. M. van, and Engelhard, G. H.: A decline in primary production in the North Sea over 25 years, associated with reductions in zooplankton abundance and fish stock recruitment, Glob. Change Biol., 24, e352–e364, https://doi.org/10.1111/gcb.13916, 2018.

580 Carpenter, J. R., Merckelbach, L., Callies, U., Clark, S., Gaslikova, L., and Baschek, B.: Potential Impacts of Offshore Wind Farms on North Sea Stratification, PLOS ONE, 11, e0160830, https://doi.org/10.1371/journal.pone.0160830, 2016.

Carranza, M. M., Gille, S. T., Franks, P. J. S., Johnson, K. S., Pinkel, R., and Girton, J. B.: When Mixed Layers Are Not Mixed. Storm-Driven Mixing and Bio-optical Vertical Gradients in Mixed Layers of the Southern
585 Ocean, J. Geophys. Res. Oceans, 123, 7264–7289, https://doi.org/10.1029/2018JC014416, 2018.

Carvalho, F., Kohut, J., Oliver, M. J., and Schofield, O.: Defining the ecologically relevant mixed-layer depth for Antarctica's coastal seas, Geophys. Res. Lett., 44, 338–345, https://doi.org/10.1002/2016GL071205, 2017.

Chiswell, S. M.: Annual cycles and spring blooms in phytoplankton: don't abandon Sverdrup completely,
590 Mar. Ecol. Prog. Ser., 443, 39–50, https://doi.org/10.3354/meps09453, 2011.

Chu, P. C. and Fan, C.: Maximum angle method for determining mixed layer depth from seaglider data, J. Oceanogr., 67, 219–230, https://doi.org/10.1007/s10872-011-0019-2, 2011.

Chu, P. C. and Fan, C.: Global ocean synoptic thermocline gradient, isothermal-layer depth, and other upper ocean parameters, Sci. Data, 6, 119, https://doi.org/10.1038/s41597-019-0125-3, 2019.

595 Costa, R. R., Mendes, C. R. B., Tavano, V. M., Dotto, T. S., Kerr, R., Monteiro, T., Odebrecht, C., and Secchi, E. R.: Dynamics of an intense diatom bloom in the Northern Antarctic Peninsula, February 2016, Limnol. Oceanogr., 65, 2056–2075, https://doi.org/10.1002/lno.11437, 2020.

Courtois, P., Hu, X., Pennelly, C., Spence, P., and Myers, P. G.: Mixed layer depth calculation in deep convection regions in ocean numerical models, Ocean Model., 120, 60–78, https://doi.org/10.1016/j.ocemod.2017.10.007, 2017.

Cullen, J. J.: Subsurface Chlorophyll Maximum Layers: Enduring Enigma or Mystery Solved?, Annu. Rev. Mar. Sci., 7, 207–239, https://doi.org/10.1146/annurev-marine-010213-135111, 2015.

Dave, A. C. and Lozier, M. S.: Examining the global record of interannual variability in stratification and marine productivity in the low-latitude and mid-latitude ocean, J. Geophys. Res. Oceans, 118, 3114–3127, https://doi.org/10.1002/jgrc.20224, 2013.

Dave, A. C. and Lozier, M. S.: The impact of advection on stratification and chlorophyll variability in the equatorial Pacific, Geophys. Res. Lett., 42, 4523–4531, https://doi.org/10.1002/2015GL063290, 2015.

De Dominicis, M., Wolf, J., and O'Hara Murray, R.: Comparative Effects of Climate Change and Tidal Stream Energy Extraction in a Shelf Sea, J. Geophys. Res. Oceans, 123, 5041–5067, https://doi.org/10.1029/2018JC013832, 2018.

Detoni, A. M. S., de Souza, M. S., Garcia, C. A. E., Tavano, V. M., and Mata, M. M.: Environmental conditions during phytoplankton blooms in the vicinity of James Ross Island, east of the Antarctic Peninsula, Polar Biol., 38, 1111–1127, https://doi.org/10.1007/s00300-015-1670-7, 2015.

Diehl, S.: Phytoplankton, Light, and Nutrients in a Gradient of Mixing Depths: Theory, Ecology, 83, 386–398, https://doi.org/10.1890/0012-9658(2002)083[0386:PLANIA]2.0.CO;2, 2002.

Diehl, S., Berger, S., Ptacnik, R., and Wild, A.: Phytoplankton, Light, and Nutrients in a Gradient of Mixing Depths: Field Experiments, Ecology, 83, 399–411, https://doi.org/10.1890/0012-9658(2002)083[0399:PLANIA]2.0.CO;2, 2002.

Dorrell, R. M., Lloyd, C. J., Lincoln, B. J., Rippeth, T. P., Taylor, J. R., Caulfield, C. P., Sharples, J., Polton, J. A., Scannell, B. D., Greaves, D. M., Hall, R. A., and Simpson, J. H.: Anthropogenic Mixing in Seasonally Stratified Shelf Seas by Offshore Wind Farm Infrastructure, Front. Mar. Sci., 9, 2022.

D'Ortenzio, F., Lavigne, H., Besson, F., Claustre, H., Coppola, L., Garcia, N., Laës-Huon, A., Le Reste, S., Malardé, D., Migon, C., Morin, P., Mortier, L., Poteau, A., Prieur, L., Raimbault, P., and Testor, P.: Observing mixed layer depth, nitrate and chlorophyll concentrations in the northwestern Mediterranean: A combined satellite and NO$_3$ profiling floats experiment, Geophys. Res. Lett., 41, 6443–6451, https://doi.org/10.1002/2014GL061020, 2014.

Ducklow, H. W., Baker, K., Martinson, D. G., Quetin, L. B., Ross, R. M., Smith, R. C., Stammerjohn, S. E., Vernet, M., and Fraser, W.: Marine pelagic ecosystems: the West Antarctic Peninsula, Philos. Trans. R. Soc. B Biol. Sci., 362, 67–94, https://doi.org/10.1098/rstb.2006.1955, 2007.

Durán-Campos, E., Monreal-Gómez, M. A., Salas de León, D. A., and Coria-Monter, E.: Chlorophyll-a vertical distribution patterns during summer in the Bay of La Paz, Gulf of California, Mexico, Egypt. J. Aquat. Res., 45, 109–115, https://doi.org/10.1016/j.ejar.2019.04.003, 2019.

Durski, S. M., Glenn, S. M., and Haidvogel, D. B.: Vertical mixing schemes in the coastal ocean: Comparison of the level 2.5 Mellor-Yamada scheme with an enhanced version of the K profile parameterization, J. Geophys. Res. Oceans, 109, https://doi.org/10.1029/2002JC001702, 2004.

Erickson, Z. K., Thompson, A. F., Cassar, N., Sprintall, J., and Mazloff, M. R.: An advective mechanism for deep chlorophyll maxima formation in southern Drake Passage, Geophys. Res. Lett., 43, 10,846-10,855, https://doi.org/10.1002/2016GL070565, 2016.

Gielen, D., Gorini, R., Wagner, N., Leme, R., Gutierrez, L., Prakash, G., Asmelash, E., Janeiro, L., Gallina, G., Vale, G., Sani, L., Casals, X. G., Ferroukhi, R., Parajuli, B., Feng, J., Alexandri, E., Chewpreecha, U., Goldman, M., Heald, S., Stenning, J., Pollitt, H., García-Baños, C., and Renner, M.: Global energy Transformation: A Roadmap to 2050, 2019.

Glorioso, P. D. and Simpson, J. H.: Numerical modelling of the M2 tide on the northern Patagonian Shelf, Cont. Shelf Res., 14, 267–278, https://doi.org/10.1016/0278-4343(94)90016-7, 1994.

González-Pola, C., Fernández-Díaz, J. M., and Lavín, A.: Vertical structure of the upper ocean from profiles fitted to physically consistent functional forms, Deep Sea Res. Part Oceanogr. Res. Pap., 54, 1985–2004, https://doi.org/10.1016/j.dsr.2007.08.007, 2007.

Gradone, J. C., Oliver, M. J., Davies, A. R., Moffat, C., and Irwin, A.: Sea Surface Kinetic Energy as a Proxy for Phytoplankton Light Limitation in the Summer Pelagic Southern Ocean, J. Geophys. Res. Oceans, 125, e2019JC015646, https://doi.org/10.1029/2019JC015646, 2020.

Hickman, A., Moore, C., Sharples, J., Lucas, M., Tilstone, G., Krivtsov, V., and Holligan, P.: Primary production and nitrate uptake within the seasonal thermocline of a stratified shelf sea, Mar. Ecol. Prog. Ser., 463, 39–57, https://doi.org/10.3354/meps09836, 2012.

Höfer, J., Giesecke, R., Hopwood, M. J., Carrera, V., Alarcón, E., and González, H. E.: The role of water column stability and wind mixing in the production/export dynamics of two bays in the Western Antarctic Peninsula, Prog. Oceanogr., 174, 105–116, https://doi.org/10.1016/j.pocean.2019.01.005, 2019.

Holligan, P. M., Balch, W. M., and Yentsch, C. M.: The significance of subsurface chlorophyll, nitrite and ammonium maxima in relation to nitrogen for phytoplankton growth in stratified waters of the Gulf of Maine, J. Mar. Res., 42, 1051–1073, https://doi.org/10.1357/002224084788520747, 1984.

Holte, J. and Talley, L.: A New Algorithm for Finding Mixed Layer Depths with Applications to Argo Data and Subantarctic Mode Water Formation, J. Atmospheric Ocean. Technol., 26, 1920–1939, https://doi.org/10.1175/2009JTECHO543.1, 2009.

Kara, A. B., Rochford, P. A., and Hurlburt, H. E.: An optimal definition for ocean mixed layer depth, J. Geophys. Res. Oceans, 105, 16803–16821, https://doi.org/10.1029/2000JC900072, 2000.

Klymak, J. M., Pinkel, R., and Rainville, L.: Direct Breaking of the Internal Tide near Topography: Kaena Ridge, Hawaii, J. Phys. Oceanogr., 38, 380–399, https://doi.org/10.1175/2007JPO3728.1, 2008.

Lande, R. and Wood, A. M.: Suspension times of particles in the upper ocean, Deep Sea Res. Part Oceanogr. Res. Pap., 34, 61–72, https://doi.org/10.1016/0198-0149(87)90122-1, 1987.

Lee, Z., Marra, J., Perry, M. J., and Kahru, M.: Estimating oceanic primary productivity from ocean color remote sensing: A strategic assessment, J. Mar. Syst., 149, 50–59, https://doi.org/10.1016/j.jmarsys.2014.11.015, 2015.

Leeuwen, S. van, Tett, P., Mills, D., and Molen, J. van der: Stratified and nonstratified areas in the North Sea: Long-term variability and biological and policy implications, J. Geophys. Res. Oceans, 120, 4670–4686, https://doi.org/10.1002/2014JC010485, 2015.

Lips, U., Lips, I., Liblik, T., and Kuvaldina, N.: Processes responsible for the formation and maintenance of sub-surface chlorophyll maxima in the Gulf of Finland, Estuar. Coast. Shelf Sci., 88, 339–349, https://doi.org/10.1016/j.ecss.2010.04.015, 2010.

Loder, J. W., Brickman, D., and Horne, E. P. W.: Detailed structure of currents and hydrography on the northern side of Georges Bank, J. Geophys. Res. Oceans, 97, 14331–14351, https://doi.org/10.1029/92JC01342, 1992.

Lorbacher, K., Dommenget, D., Niiler, P. P., and Köhl, A.: Ocean mixed layer depth: A subsurface proxy of ocean-atmosphere variability, J. Geophys. Res. Oceans, 111, https://doi.org/10.1029/2003JC002157, 2006.

Lozier, M. S., Dave, A. C., Palter, J. B., Gerber, L. M., and Barber, R. T.: On the relationship between stratification and primary productivity in the North Atlantic, Geophys. Res. Lett., 38, https://doi.org/10.1029/2011GL049414, 2011.

Martin, J., Tremblay, J.-É., Gagnon, J., Tremblay, G., Lapoussière, A., Jose, C., Poulin, M., Gosselin, M., Gratton, Y., and Michel, C.: Prevalence, structure and properties of subsurface chlorophyll maxima in Canadian Arctic waters, Mar. Ecol. Prog. Ser., 412, 69–84, https://doi.org/10.3354/meps08666, 2010.

van der Molen, J., Smith, H. C. M., Lepper, P., Limpenny, S., and Rees, J.: Predicting the large-scale consequences of offshore wind turbine array development on a North Sea ecosystem, Cont. Shelf Res., 85, 60–72, https://doi.org/10.1016/j.csr.2014.05.018, 2014.

Montégut, C. de B., Madec, G., Fischer, A. S., Lazar, A., and Iudicone, D.: Mixed layer depth over the global ocean: An examination of profile data and a profile-based climatology, J. Geophys. Res. Oceans, 109, https://doi.org/10.1029/2004JC002378, 2004.

Montes-Hugo, M., Doney, S. C., Ducklow, H. W., Fraser, W., Martinson, D., Stammerjohn, S. E., and Schofield, O.: Recent Changes in Phytoplankton Communities Associated with Rapid Regional Climate Change Along the Western Antarctic Peninsula, Science, 323, 1470–1473, https://doi.org/10.1126/science.1164533, 2009.

Orihuela-Pinto, B., England, M. H., and Taschetto, A. S.: Interbasin and interhemispheric impacts of a collapsed Atlantic Overturning Circulation, Nat. Clim. Change, 12, 558–565, https://doi.org/10.1038/s41558-022-01380-y, 2022.

Pingree, R. D., Holligan, P. M., Mardell, G. T., and Harris, R. P.: Vertical distribution of plankton in the skagerrak in relation to doming of the seasonal thermocline, Cont. Shelf Res., 1, 209–219, https://doi.org/10.1016/0278-4343(82)90005-X, 1982.

Prend, C. J., Gille, S. T., Talley, L. D., Mitchell, B. G., Rosso, I., and Mazloff, M. R.: Physical Drivers of Phytoplankton Bloom Initiation in the Southern Ocean's Scotia Sea, J. Geophys. Res. Oceans, 124, 5811–5826, https://doi.org/10.1029/2019JC015162, 2019.

Prézelin, B. B., Hofmann, E. E., Mengelt, C., and Klinck, J. M.: The linkage between Upper Circumpolar Deep Water (UCDW) and phytoplankton assemblages on the west Antarctic Peninsula continental shelf, J. Mar. Res., 58, 165–202, https://doi.org/10.1357/002224000321511133, 2000.

Prézelin, B. B., Hofmann, E. E., Moline, M., and Klinck, J. M.: Physical forcing of phytoplankton community structure and primary production in continental shelf waters of the Western Antarctic Peninsula, J. Mar. Res., 62, 419–460, https://doi.org/10.1357/0022240041446173, 2004.

Richardson, K. and Bendtsen, J.: Vertical distribution of phytoplankton and primary production in relation to nutricline depth in the open ocean, Mar. Ecol. Prog. Ser., 620, 33–46, https://doi.org/10.3354/meps12960, 2019.

Richardson, K. and Pedersen, F. B.: Estimation of new production in the North Sea: consequences for temporal and spatial variability of phytoplankton, ICES J. Mar. Sci., 55, 574–580, https://doi.org/10.1006/jmsc.1998.0402, 1998.

720 Rosenberg, R., Dahl, E., Edler, L., Fyrberg, L., Granéli, E., Granéli, W., Hagström, Å., Lindahl, O., Matos, M. O., Pettersson, K., Sahlsten, E., Tiselius, P., Turk, V., and Wikner, J.: Pelagic nutrient and energy transfer during spring in the open and coastal Skagerrak, Mar. Ecol. Prog. Ser., 61, 215–231, 1990.

Ross, O. N. and Sharples, J.: Phytoplankton motility and the competition for nutrients in the thermocline, Mar. Ecol. Prog. Ser., 347, 21–38, https://doi.org/10.3354/meps06999, 2007.

725 Ryan-Keogh, T. J. and Thomalla, S. J.: Deriving a Proxy for Iron Limitation From Chlorophyll Fluorescence on Buoyancy Gliders, Front. Mar. Sci., 7, 275, https://doi.org/10.3389/fmars.2020.00275, 2020.

Schmidt, K., Birchill, A. J., Atkinson, A., Brewin, R. J. W., Clark, J. R., Hickman, A. E., Johns, D. G., Lohan, M. C., Milne, A., Pardo, S., Polimene, L., Smyth, T. J., Tarran, G. A., Widdicombe, C. E., Woodward, E. M. S., and Ussher, S. J.: Increasing picocyanobacteria success in shelf waters contributes to long-term food web

730 degradation, Glob. Change Biol., https://doi.org/10.1111/gcb.15161, 2020.

Schofield, O., Miles, T., Alderkamp, A.-C., Lee, S., Haskins, C., Rogalsky, E., Sipler, R., Sherrell, R. M., and Yager, P. L.: *In situ* phytoplankton distributions in the Amundsen Sea Polynya measured by autonomous gliders, Elem. Sci. Anthr., 3, 000073, https://doi.org/10.12952/journal.elementa.000073, 2015.

Schulien, J. A., Behrenfeld, M. J., Hair, J. W., Hostetler, C. A., and Twardowski, M. S.: Vertically- resolved
735 phytoplankton carbon and net primary production from a high spectral resolution lidar, Opt. Express, 25, 13577, https://doi.org/10.1364/OE.25.013577, 2017.

Schultze, L. K. P., Merckelbach, L. M., Horstmann, J., Raasch, S., and Carpenter, J. R.: Increased Mixing and Turbulence in the Wake of Offshore Wind Farm Foundations, J. Geophys. Res. Oceans, 125, e2019JC015858, https://doi.org/10.1029/2019JC015858, 2020.

740 Scott, B. E., Sharples, J., Ross, O. N., Wang, J., Pierce, G. J., and Camphuysen, C. J.: Sub-surface hotspots in shallow seas: fine-scale limited locations of top predator foraging habitat indicated by tidal mixing and sub-surface chlorophyll, Mar. Ecol. Prog. Ser., 408, 207–226, https://doi.org/10.3354/meps08552, 2010.

Sharples, J., Moore, M. C., Rippeth, T. P., Holligan, P. M., Hydes, D. J., Fisher, N. R., and Simpson, J. H.: Phytoplankton distribution and survival in the thermocline, Limnol. Oceanogr., 46, 486–496,
745 https://doi.org/10.4319/lo.2001.46.3.0486, 2001.

Sharples, J., Ross, O. N., Scott, B. E., Greenstreet, S. P. R., and Fraser, H.: Inter-annual variability in the timing of stratification and the spring bloom in the North-western North Sea, Cont. Shelf Res., 26, 733–751, https://doi.org/10.1016/j.csr.2006.01.011, 2006.

Sharples, J., Scott, B. E., and Inall, M. E.: From physics to fishing over a shelf sea bank, Prog. Oceanogr., 117,
750 1–8, https://doi.org/10.1016/j.pocean.2013.06.015, 2013.

Silva, E., Counillon, F., Brajard, J., Korosov, A., Pettersson, L. H., Samuelsen, A., and Keenlyside, N.: Twenty-One Years of Phytoplankton Bloom Phenology in the Barents, Norwegian, and North Seas, Front. Mar. Sci., 8, 2021.

Simpson, J., Hughes, D. G., and Morris, N. C. G.: The relation of seasonal stratification to tidal mixing on the
755 continental shelf, Deep-Sea Res., 327–340, 1980.

Somavilla, R., González-Pola, C., and Fernández-Diaz, J.: The warmer the ocean surface, the shallower the mixed layer. How much of this is true?, J. Geophys. Res. Oceans, 122, 7698–7716, https://doi.org/10.1002/2017JC013125, 2017.

Steinacher, M., Joos, F., Frölicher, T. L., Bopp, L., Cadule, P., Cocco, V., Doney, S. C., Gehlen, M., Lindsay, K., Moore, J. K., Schneider, B., and Segschneider, J.: Projected 21st century decrease in marine productivity: a multi-model analysis, Biogeosciences, 7, 979–1005, https://doi.org/10.5194/bg-7-979-2010, 2010.

Taboada, F. G. and Anadón, R.: Patterns of change in sea surface temperature in the North Atlantic during the last three decades: beyond mean trends, Clim. Change, 115, 419–431, https://doi.org/10.1007/s10584-012-0485-6, 2012.

Takahashi, M. and Hori, T.: Abundance of picophytoplankton in the subsurface chlorophyll maximum layer in subtropical and tropical waters, Mar. Biol., 79, 177–186, https://doi.org/10.1007/BF00951826, 1984.

Therriault, J.-C., Lawrence, D. J., and Piatt, T.: Spatial variability of phytoplankton turnover in relation to physical processes in a coastal environment, Limnol. Oceanogr., 23, 900–911, https://doi.org/10.4319/lo.1978.23.5.0900, 1978.

Thomson, R. E. and Fine, I. V.: Estimating Mixed Layer Depth from Oceanic Profile Data, J. Atmospheric Ocean. Technol., 20, 319–329, https://doi.org/10.1175/1520-0426(2003)020<0319:EMLDFO>2.0.CO;2, 2003.

Trifonova, N. I., Scott, B. E., De Dominicis, M., Waggitt, J. J., and Wolf, J.: Bayesian network modelling provides spatial and temporal understanding of ecosystem dynamics within shallow shelf seas, Ecol. Indic., 129, 107997, https://doi.org/10.1016/j.ecolind.2021.107997, 2021.

Walsby, A. E.: Numerical integration of phytoplankton photosynthesis through time and depth in a water column, New Phytol., 136, 189–209, https://doi.org/10.1046/j.1469-8137.1997.00736.x, 1997.

Warton, D. I., Wright, I. J., Falster, D. S., and Westoby, M.: Bivariate line-fitting methods for allometry, Biol. Rev., 81, 259–291, https://doi.org/10.1017/S1464793106007007, 2006.

Weston, K., Fernand, L., Mills, D. K., Delahunty, R., and Brown, J.: Primary production in the deep chlorophyll maximum of the central North Sea, J. Plankton Res., 27, 909–922, https://doi.org/10.1093/plankt/fbi064, 2005.

Yentsch, C. S.: Influence of geostrophy on primary production. [Effect of ocean currents on nutrients of ocean water], Tethys Fr., 6:1–2, 1974.

Yentsch, C. S.: Phytoplankton Growth in the Sea, in: Primary Productivity in the Sea, edited by: Falkowski, P. G., Springer US, Boston, MA, 17–32, https://doi.org/10.1007/978-1-4684-3890-1_2, 1980.

Zhang, W.-Z., Wang, H., Chai, F., and Qiu, G.: Physical drivers of chlorophyll variability in the open South China Sea, J. Geophys. Res. Oceans, 121, 7123–7140, https://doi.org/10.1002/2016JC011983, 2016.

Zhao, C., Maerz, J., Hofmeister, R., Röttgers, R., Wirtz, K., Riethmüller, R., and Schrum, C.: Characterizing the vertical distribution of chlorophyll a in the German Bight, Cont. Shelf Res., 175, 127–146, https://doi.org/10.1016/j.csr.2019.01.012, 2019a.

Zhao, C., Daewel, U., and Schrum, C.: Tidal impacts on primary production in the North Sea, Earth Syst. Dyn., 10, 287–317, https://doi.org/10.5194/esd-10-287-2019, 2019b.